Nigerian Journal of Applied Physics (NJAP)
ISSN Print: 3115-5871
ISSN Online: 3115-588X
DOI: https://doi.org/10.62292/njap-v2i3-2026-94
Volume 2(3), September 2026

Simulation Of Quantum Spin Systems For Qubit Applications

Iyanuoluwa Olaniyi Ajayi

Department of Physics, Bamidele Olumilua University of Education, Science and Technology, Ikere Ekiti, Ekiti State, Nigeria.

*Corresponding author's email: ajayi.iyanuoluwa@bouesti.edu.ng Phone: +2347031463948
ORCiD No: https://orcid.org/0009-0008-6399-0167

ABSTRACT

This study presents a numerical investigation of the dynamics of two coupled spin-1/2 quantum systems with emphasis on entanglement, quantum coherence, and state fidelity. The system is described by an isotropic Heisenberg Hamiltonian and investigated for exchange-coupling strengths J=−1, −0.5, 0, 0.5, and 11. Four representative initial states, comprising the Bell state, a partially entangled state with initial concurrence C (0) =0.8, and the separable states |01⟩and |++⟩are considered. Closed-system evolution is obtained using the unitary propagator, while environmental effects are modelled through a Lindblad master equation with local Markovian pure-dephasing channels for γ=0,0.1,0.5, and 11. The results show that the Bell state maintains maximal concurrence under closed Heisenberg evolution, while the partially entangled state retains its initial concurrence of 0.8 for all tested exchange couplings. In contrast, the initially separable |01⟩state develops strong transient entanglement through exchange interaction, reaching concurrence values essentially equal to unity for |J|=0.5 and 11, whereas the |++⟩state remains separable to numerical precision. Under pure dephasing, concurrence and coherence decay progressively with increasing dephasing strength, while fidelity decreases toward its asymptotic value. The numerical calculations were further validated through normalization and Hermiticity checks, analytical dephasing benchmarks, and step-refinement convergence tests, with discrepancies remaining at machine-precision levels. The findings demonstrate that the preservation and generation of quantum correlations depend strongly on the initial state, exchange interaction, and environmental decoherence, providing validated numerical benchmarks for the study of coupled qubit dynamics.

Keywords:
Heisenberg Interaction,
Quantum Entanglement,
Pure Dephasing,
Concurrence,
Qubit Dynamics.

INTRODUCTION

Quantum computing is an important area of contemporary physics and computational research because quantum systems can exploit superposition, interference, and entanglement to perform information-processing tasks that are difficult to reproduce efficiently with classical systems (Nielsen and Chuang 2010; Preskill 2018). Quantum bits (qubits) are two-level quantum systems whose basis states are commonly denoted by |0⟩ and |1⟩. Spin-1/2 particles provide natural two-level systems and are therefore relevant physical platforms for qubit implementation and quantum information processing (Sachdev, 2011). Spin Hamiltonians such as the Ising and Heisenberg models are widely used to describe interactions among quantum spins and to investigate their collective dynamics (Heisenberg 1928; Sachdev, 2011). The isotropic Heisenberg model is particularly useful for studying coupled qubits because it provides a tractable description of exchange-mediated spin interactions. Quantum coherence is essential for maintaining superposition and quantum correlations, whereas interaction with the environment can produce decoherence and degrade these resources (Chirolli and Burkard, 2008; Schlosshauer, 2019). Recent developments in numerical quantum simulation have made it possible to investigate quantum-state evolution, spin interactions, entanglement, and decoherence without requiring direct access to experimental quantum hardware (Gebhart et al., 2023; Morsch et al., 2025). In this study, the isotropic Heisenberg Hamiltonian is used to examine single- and two-qubit dynamics, while a Lindblad master-equation model is used to investigate environmental

dephasing. The study therefore focuses on the evolution and stability of quantum states, entanglement, coherence, and fidelity under controlled interaction and decoherence conditions. The isotropic Heisenberg interaction's Hamiltonian is given by:

$H=-J\sum_{\langle i,j\rangle}(\sigma_i^x\sigma_j^x+\sigma_i^y\sigma_j^y+\sigma_i^z\sigma_j^z)$

Where J represents the spin coupling strength and are the Pauli spin matrices. The behavior of connected qubit system is determined by quantum states evolution under this Hamiltonian. Quantum coherence remains one of the most important prerequisite for a trustworthy quantum computation. However, interactions with external surroundings can produce decoherence in practical quantum systems, this decoherence destroys quantum superposition and entanglement (Chirolli and Burkard, 2008; Schlosshauer, 2019). An important area of studying in quantum information science and condensed matter physics is the coherent dynamics of Spin base qubit system (Lutchyn et al., 2008). Therefore the quantum spin system cannot be totally studied without the need of costly experimental quantum apparatus because of recent technological development in computational and numerical quantum simulations. The quantum states evolution and spin coherence behavior and entanglement dynamics can now be frequently studied using numerical simulations which are based on matrix mechanics time dependence Schrodinger evolution equations and density operators (Morsch et al., 2025; Gebhart et al., 2023). These methods are important since noise, decoherence and instability are technological construct on contemporary quantum processes as noted by Preskill, 2018). Numerical simulations of Spin 1/2 Hamiltonians with employed in this research to give a computational examination of quantum spin system especially in qubit applications. The research focus on simulating the entanglement dynamics, Spin interaction, decoherence behavior and the quantum state development in coupled quantum bit systems. The result of this story is expected to support current investigations in the computational condensed metter physics especially in quantum computing and quantum materials. The aim of this research is to use the Hamiltonian best quantum mechanical models to simulate spin 1/2 quantum states, quantum coherence, Spin interactions and the entanglement dynamics so as to computationally study quantum spin systems. The research will examine the development and stability of source system most especially under control spin interaction, this shows if quantum bit systems are suitable for quantum computing and quantum information processing application.

Accordingly, the objectives of this study are:

i. To simulate the unitary evolution of coupled spin-1/2 qubits;
ii. To investigate entanglement dynamics under the isotropic Heisenberg Hamiltonian;
iii. To examine the effects of pure dephasing on quantum coherence, concurrence, and fidelity;
iv. To investigate the combined influence of exchange coupling and decoherence; and
v. To identify parameter regimes that preserve quantum correlations.

MATERIALS AND METHODS

This study adopts a computational quantum-mechanical approach to investigate spin-1/2 quantum systems for qubit applications. The numerical calculations were performed in Python, while MATLAB was used only for visualization of the resulting simulation data. The computational procedure consisted of constructing the qubit state vectors and Pauli operators, forming the two-qubit Heisenberg Hamiltonian through Kronecker products, propagating the quantum states under unitary evolution, and solving the Lindblad master equation for the open-system calculations. The first stage of the simulation was the mathematical representation of a qubit as a two-level quantum system, defined as:

$$|0\rangle = \begin{pmatrix}1\\0\end{pmatrix}, \qquad |1\rangle = \begin{pmatrix}0\\1\end{pmatrix}$$

While a general qubit state is represented as

$$|\psi\rangle = \alpha|0\rangle + \beta|1\rangle$$

Subject to the normalization condition

$$|\alpha|^2 + |\beta|^2 = 1$$

Where α *and* β are complex probability amplitudes. Quantum superposition states were generated numerically by assigning different values to the coefficientsα *and* β. Equal superposition states were constructed using:

$$|\psi\rangle = \frac{1}{\sqrt{2}}(|0\rangle + |1\rangle)$$

Which is a balanced qubit configuration.

The spin properties of the qubit systems were described using the Pauli spin matrices given by

$$\sigma_x = \begin{pmatrix}0 & 1\\1 & 0\end{pmatrix}$$

$$\sigma_y = \begin{pmatrix}0 & -i\\i & 0\end{pmatrix}$$

$$\sigma_z = \begin{pmatrix}1 & 0\\0 & -1\end{pmatrix}$$

The Pauli matrices describe spin measurements and rotations along the x-, y-, and z-directions, respectively. For the two-qubit system, operators acting on individual qubits were constructed with Kronecker products, The isotropic nearest-neighbour Heisenberg Hamiltonian was used to model the interaction between the two qubits. The sign convention adopted throughout the revised analysis is the one explicitly defined by the Hamiltonian below; the physical interpretation of positive and negative J is therefore tied to this convention and is not changed independently in the Results section.

$$H = -J\sum_{\langle i,j\rangle}(\sigma_i^x\sigma_j^x + \sigma_i^y\sigma_j^y + \sigma_i^z\sigma_j^z)$$

$(\sigma_k^{(i)})$ Denotes the Pauli operator in the (k)-direction acting on the (i)-th qubit, while (J) represents the exchange-coupling parameter. The simulations has the parameter set

J = −1.0, −0.5, 0, 0.5, and 1.0 so that both signs and the uncoupled case can be compared. The sign of J is interpreted strictly according to the Hamiltonian convention adopted above.

$[H = -\frac{J}{4}(\sigma_x \otimes \sigma_x + \sigma_y \otimes \sigma_y + \sigma_z \otimes \sigma_z)]$

J is the exchange coupling between spin operators $S_i = \sigma_i/2$.

The time-dependent Schrödinger equation governs the closed-system evolution. For a time-independent Hamiltonian, the formal solution is evaluated directly through the unitary propagator rather than by repeatedly applying a finite difference approximation. This provides a numerically stable reference solution against which any time-integration procedure used for the open system can be checked.

$i\hbar \frac{\partial}{\partial t}|\psi(t)\rangle = H|\psi(t)\rangle$

The unitary evolution operator is obtained from the matrix exponential of the Hamiltonian. For each requested time t, the evolved state is generated from U (t)|ψ(0)⟩. The matrix exponential is evaluated numerically with a verified matrix-exponential routine in the Python scientific-computing environment.

$|\psi(t)\rangle = e^{-iHt/\hbar}|\psi(0)\rangle$

The unitary evolution operator

$U(t) = e^{-iHt/\hbar}$

For the calculations, the closed-system states were evaluated over the time interval$0 \leq t \leq 20$, with 1001 solution points reported. The corresponding output-point spacing was calculated as

$\Delta t_{\text{out}} = \frac{t_{\text{final}} - t_{\text{initial}}}{N-1} = \frac{20-0}{1001-1} = 0.02$

Time units. It is important to note that 0.02 represents the spacing between the reported solution points and should not be interpreted as the internal integration step size of the adaptive Lindblad solver. The Bell states and other two-qubit initial states were propagated using the same Hamiltonian protocol to ensure consistency across the calculations.

$|\Phi^+\rangle = \frac{1}{\sqrt{2}}(|00\rangle + |11\rangle)$

To test the dependence of entanglement dynamics on the initial state, partially entangled states of the form shown below were included in addition to the maximally entangled Bell state. The parameter p was varied over the values reported in the Results section, with p = 0.5 corresponding to maximal entanglement and p = 0 or 1 corresponding to separable limiting states.

$|\psi(p)\rangle = \sqrt{p}|00\rangle + \sqrt{1-p}|11\rangle,$

For each initial state, the concurrence was evaluated from the evolved two-qubit density matrix. The partially entangled-state calculations were repeated over the selected J values and the resulting time-dependent concurrence was compared with its analytically determined initial value C(0) = 2√[p(1−p)]. The density matrices and reduced states were retained at every reported time point so that entanglement dynamics could be calculated consistently from the same numerical states used for the other observables. Open-system calculations were formulated in the density-matrix representation. For a pure initial state, the density operator is constructed as ρ(0) = |ψ(0)⟩⟨ψ(0)|. The density matrix is evolved with the Lindblad master equation given below.

$\rho = |\psi\rangle\langle\psi|$

The Lindblad equation was treated as a Markovian pure-dephasing model. For the revised implementation, the effective dephasing rate γ is defined so that the selected coherence component decays as exp(−γt) in the uncoupled reference case. The corresponding collapse operator is defined explicitly in the numerical implementation so that the decay-rate convention is unambiguous. The master equation is integrated numerically with a controlled adaptive ODE solver, and the solution is evaluated at the same output times used for comparison of the observables.

$\frac{d\rho}{dt} = -\frac{i}{\hbar}[H, \rho] + \mathrm{L}(\rho)$

Here, L is the collapse operator representing the specified pure-dephasing channel. The open-system calculation is performed for γ = 0.0, 0.1, 0.5, and 1.0. The γ = 0 case is also used as a closed-system consistency check. At each reported time, the trace of ρ is evaluated to verify normalization, and the Hermiticity of ρ is checked numerically. As part of the numerical validation, the maximum deviation of the density-matrix trace from unity was monitored throughout the simulation. This quantity was defined as

$\delta_{\text{Tr}} = \max_t |Tr[\rho(t)] - 1|$

The value of δ_{Tr} was recorded to assess the preservation of the normalization condition $Tr[\rho(t)] = 1$ during the numerical evolution.

$\langle O\rangle = \langle\psi|O|\psi\rangle$

Where O denotes a quantum observable, such as a Pauli operator. The expectation values are used to characterize spin orientation and dynamics. Quantum-state fidelity is calculated between the evolved state and the specified reference state using the fidelity definition given below. For a pure reference state, the implementation is checked against the corresponding pure-state expression so that the numerical and analytical definitions are consistent.

$F(t) = \langle\psi_{\text{ref}}|\rho(t)|\psi_{\text{ref}}\rangle.$

The fidelity lies between zero and one, with F = 1 indicating exact agreement with the reference state. To examine the joint influence of exchange coupling and environmental dephasing, J and γ are varied systematically over the parameter sets stated above. For every parameter combination, the same state-construction, propagation, and observable- calculation procedures are used. The revised analysis also includes numerical convergence and error checks before final values are reported.

$x = \langle\sigma_x, y = \langle\sigma_y, z = \langle\sigma_z\rangle$

The numerical protocol for the revised study is as follows. The basis states and Pauli operators are constructed in double-precision arithmetic. The Hamiltonian is assembled from Kronecker products and verified to be Hermitian. Closed-system evolution is obtained from $U(t) = e^{-iHt}$ with the matrix exponential evaluated numerically. The open-system density matrix is propagated by numerical integration of the Lindblad equation using an adaptive ODE solver with specified relative and absolute tolerances. Concurrence, l1-norm coherence, expectation values, and fidelity are calculated from the resulting states. Sixth, normalization is checked through Tr(ρ)= 1 and Hermiticity is checked through ρ = ρ†. Numerical convergence is assessed by repeating representative calculations at a finer output resolution and comparing the resulting observables. The maximum absolute difference between the baseline and refined calculations is recorded as the numerical resolution error. Numerical parameter protocol: time interval t = 0–20; 1001 reported solution points; output spacing $\Delta t_{\text{out}} = \frac{20-0}{1001-1} = 0.02$, J = −1.0, −0.5, 0, 0.5, 1.0; γ = 0.0, 0.1, 0.5, 1.0. The output spacing is distinguished from the adaptive ODE solver step used for the Lindblad equation.

Computational Environment

The simulation used Python 3.13.15, NumPy 2.1.3, and SciPy 1.16.3. MATLAB is used as a visualization tool where applicable.

RESULTS AND DISCUSSION

The numerical investigation considered the isotropic two-qubit Heisenberg Hamiltonian over $0 \leq t \leq 20$. The exchange coupling was varied over J = −1.0, −0.5, 0, 0.5, and 1.0, while the local Markovian dephasing rate was varied over γ = 0, 0.1, 0.5, and 1.0. Four initial states were examined: the Bell state $|\Phi^+\rangle = |00\rangle + |11\rangle)/\sqrt{2}$, the partially entangled state $\sqrt{0.8}|00\rangle + \sqrt{0.2}|11\rangle$, and the separable states $|01\rangle$and $|{+}{+}\rangle$. The principal calculations used 1001 reported solution points, corresponding to an output spacing of Δt = 0.02. For the Lindblad evolution, the adaptive DOP 853 integrator was used with relative tolerance (rtol) = 10^{-9}, absolute tolerance (atol) = 10^{-11}, and maximum internal step 0.05. The output spacing is therefore not interpreted as the internal step size of the adaptive solver. The numerical quantities extracted from each trajectory were concurrence, l_1-norm coherence, and pure-state fidelity, with independent structural and convergence checks applied to the computed states.

Table 1: Model and Numerical Parameters

Parameter	Value
Hamiltonian	$H = -(J/4)(\sigma_x \otimes \sigma_x + \sigma_\gamma \otimes \sigma_\gamma + \sigma\_z \otimes \sigma\_z)$
Exchange coupling, J	−1, −0.5, 0, 0.5, 1
Time interval	$0 \leq t \leq 20$
Number of output points	1001
Output interval, Δt	0.02
ODE solver	DOP853
Relative tolerance, rtol	10^{-9}
Absolute tolerance, atol	10^{-11}
Maximum integration step	0.05
Dephasing rate, γ	0, 0.1, 0.5, 1
L_1	$\sqrt{(\gamma/4)}(\sigma\_z \otimes I)$
L_2	$\sqrt{(\gamma/4)}(I \otimes \sigma\_z)$
Entanglement measure	Wootters concurrence, C
Coherence measure	l_1-norm coherence
Fidelity	$F = \langle\psi|\rho|\psi\rangle$

Table 2: Initial States

Initial state	State definition	Classification	C(0)	l_1 coherence at t = 0
$\|\Phi^+\rangle$	$(\|00\rangle + \|11\rangle)/\sqrt{2}$	Maximally entangled	1.0	1.0
Partial (p = 0.8)	$\sqrt{0.8}\|00\rangle + \sqrt{0.2}\|11\rangle$	Partially entangled	0.8	0.8
$\|01\rangle$	$\|01\rangle$	Separable	0.0	0.0
$\|{+}{+}\rangle$	$\|+\rangle \otimes \|+\rangle$	Separable	0.0	3.0

The first closed-system comparison is shown in Figure 1. At J = 1, the Bell-state trajectory remains at C = 1, while the p = 0.8 state remains at C = 0.8. In contrast, the initially separable $|01\rangle$ state undergoes pronounced oscillatory entanglement generation, repeatedly approaching C = 1 before returning toward zero. The three trajectories therefore separate the roles of initial-state structure and interaction dynamics. The Bell state is an

eigenstate of the isotropic Heisenberg Hamiltonian and therefore retains its concurrence, while |01⟩ is dynamically coupled to |10⟩ and consequently develops entanglement. The p = 0.8 state does not exhibit the same interaction-induced variation in concurrence under the present Hamiltonian; its entanglement remains fixed in the closed system.

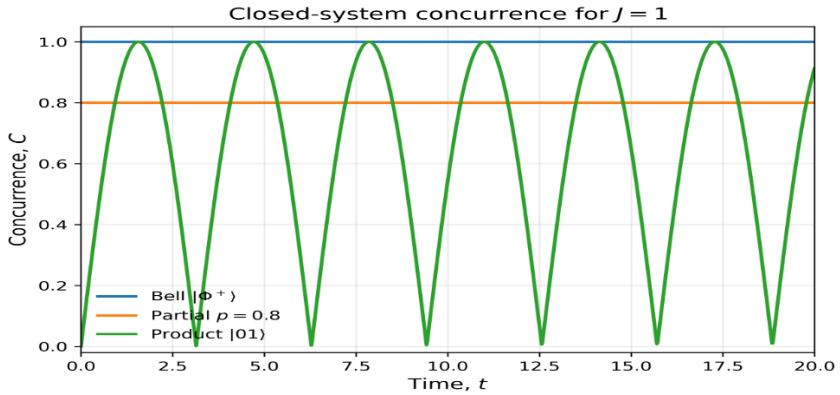

Figure 1: Closed-system concurrence for selected initial states at J = 1

The complete coupling comparison is given in Table 3. For |Φ⁺⟩, C(0) = Cmin = Cmax = C(20) = 1.0000 for all five values of J, and F(20) = 1.0000. The partially entangled p = 0.8 state similarly remains at C = 0.8000 throughout the closed-system evolution for every tested coupling, with unit final fidelity. This is a central result of the present model because the definitive calculation gives concurrence preservation at 0.8000 for the specified p = 0.8 state. The result emphasizes that concurrence preservation is state specific and should not be generalized to arbitrary partially entangled states or arbitrary exchange Hamiltonians.

Table 3: Closed-system results

Initial state	J	C(0)	Cmin	Cmax	C(20)	F(20)
|Φ⁺⟩	-1.0	1.0	1.0	1.0	1.0	1.0
|Φ⁺⟩	-0.5	1.0	1.0	1.0	1.0	1.0
|Φ⁺⟩	0.0	1.0	1.0	1.0	1.0	1.0
|Φ⁺⟩	0.5	1.0	1.0	1.0	1.0	1.0
|Φ⁺⟩	1.0	1.0	1.0	1.0	1.0	1.0
Partial (p = 0.8)	-1.0	0.8	0.8	0.8	0.8	1.0
Partial (p = 0.8)	-0.5	0.8	0.8	0.8	0.8	1.0
Partial (p = 0.8)	0.0	0.8	0.8	0.8	0.8	1.0
Partial (p = 0.8)	0.5	0.8	0.8	0.8	0.8	1.0
Partial (p = 0.8)	1.0	0.8	0.8	0.8	0.8	1.0
|01⟩	-1.0	0.0	0	0.9999992244	0.9129452452	0.704041
|01⟩	-0.5	0.0	0	0.9999996638	0.5440211109	0.080464
|01⟩	0.0	0.0	0	0	0	1.0
|01⟩	0.5	0.0	0	0.9999996638	0.5440211109	0.080464
|01⟩	1.0	0.0	0	0.9999992244	0.9129452452	0.704041
|++⟩	-1.0	1.419696×10^{-20}	1.419696×10^{-20}	1.419696×10^{-20}	1.419696×10^{-20}	1.0
|++⟩	-0.5	1.419696×10^{-20}	1.419696×10^{-20}	1.419696×10^{-20}	1.419696×10^{-20}	1.0
|++⟩	0.0	1.419696×10^{-20}	1.419696×10^{-20}	1.419696×10^{-20}	1.419696×10^{-20}	1.0
|++⟩	0.5	1.419696×10^{-20}	1.419696×10^{-20}	1.419696×10^{-20}	1.419696×10^{-20}	1.0
|++⟩	1.0	1.419696×10^{-20}	1.419696×10^{-20}	1.419696×10^{-20}	1.419696×10^{-20}	1.0

The separable |01⟩ state displays the complementary behaviour. For J = ±1, the maximum concurrence is approximately 0.999999, with C(20) = 0.912945; for J = ±0.5, C(20) = 0.544021 after reaching values very close to unity. When J = 0, the interaction is absent and C remains zero. The equal results for ±J indicate that the sign of the isotropic exchange changes the phase evolution without changing the concurrence magnitude for this initial condition. The final fidelity is 0.704041 for |J| = 1 and 0.080464 for |J| = 0.5, illustrating that strong

entanglement at intermediate times does not imply large overlap with the initial product state. The $|{+}{+}\rangle$ state remains separable to numerical precision, with concurrence of order 10^{-20} and unit final fidelity. Figure 2 shows the interaction-induced entanglement generation directly and complements the aggregate values in Table 3. The J = 0 case remains at zero concurrence throughout and is therefore not visually separated from the horizontal axis in the interaction plot.

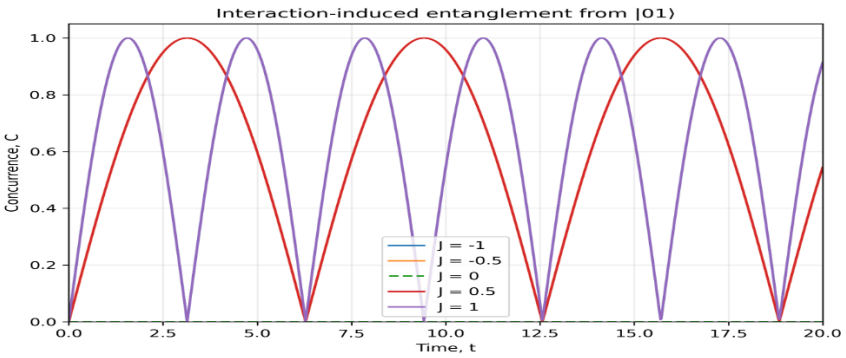

Figure 2: Interaction-induced entanglement generation from the initially separable $|01\rangle$ state for different exchange couplings

The environmental contribution was then introduced through the two local Lindblad operators specified in Table 1. For the Bell-state benchmark, the numerical dynamics have a simple analytical form: $C(t) = \exp^{-\gamma t}$, the l_1-norm coherence follows the same exponential law, and the fidelity is $F(t) = [1 + \exp^{-\gamma t}/2$. Figures 3–5 display these quantities separately. The three observables show the same ordering of decay rates: $\gamma = 0$ produces no decay, $\gamma = 0.1$ gives the slowest decay, $\gamma = 0.5$ gives rapid loss, and $\gamma = 1$ produces the fastest suppression. The agreement among the three measures is expected because, for the selected Bell state under local pure dephasing, the off-diagonal coherence is the quantity directly affected by the dissipative dynamics and is also responsible for the concurrence and the deviation of the fidelity from its asymptotic mixed-state value.

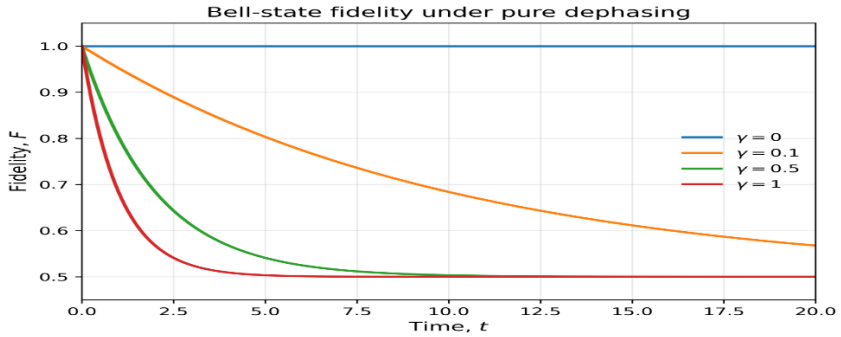

Figure 3: Bell-state fidelity under local pure dephasing for different dephasing rates

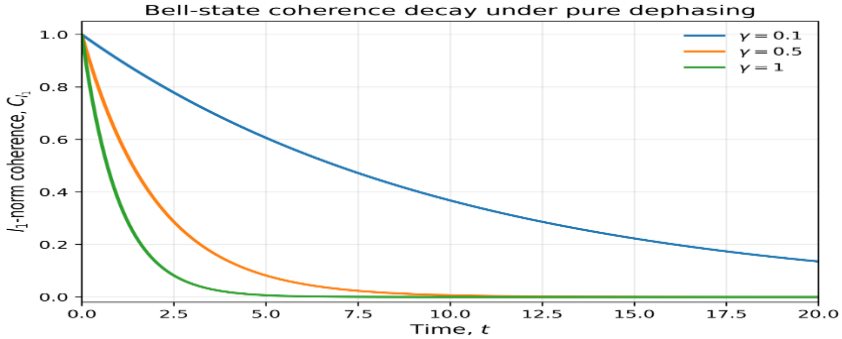

Figure 4: Bell-state l_1-norm coherence decay under local pure dephasing

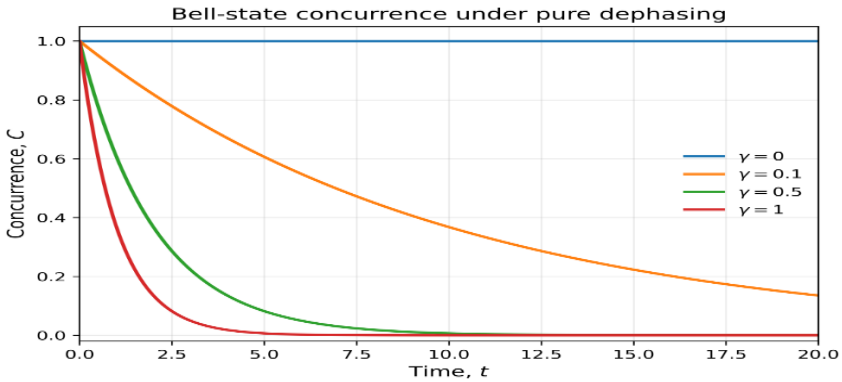

Figure 5: Bell-state concurrence decay under local pure dephasing

Table 4: Dephasing Results for $|\Phi^+\rangle$ at J = 1

γ	t	C	l_1 coherence	F
0.0	0	1.0	1.0	1.0
0.0	5	1.0	1.0	1.0
0.0	10	1.0	1.0	1.0
0.0	15	1.0	1.0	1.0
0.0	20	1.0	1.0	1.0
0.1	0	1.0	1.0	1.0
0.1	5	0.6065306597126334	0.6065306597126334	0.8032653298563167
0.1	10	0.36787944117144233	0.36787944117144233	0.6839397205857212
0.1	15	0.22313016014842982	0.22313016014842982	0.611565080074215
0.1	20	0.1353352832366127	0.1353352832366127	0.5676676416183064
0.5	0	1.0	1.0	1.0
0.5	5	0.0820849986238988	0.0820849986238988	0.5410424993119494
0.5	10	0.006737946999085467	0.006737946999085467	0.5033689734995427
0.5	15	0.0005530843701478336	0.0005530843701478336	0.5002765421850739
0.5	20	$4.5399929762484854 \times 10^{-5}$	$4.5399929762484854 \times 10^{-5}$	0.5000226999648812
1.0	0	1.0	1.0	1.0
1.0	5	0.006737946999085467	0.006737946999085467	0.5033689734995427
1.0	10	4.5399929762484854e-05	4.5399929762484854e-05	0.5000226999648812
1.0	15	3.059023205018258e-07	3.059023205018258e-07	0.5000001529511603
1.0	20	2.061153622438558e-09	2.061153622438558e-09	0.5000000010305768

Table 4 quantifies the decay represented in Figures 3–5. At $\gamma = 0$, all three quantities remain equal to their initial values. At $\gamma = 0.1$, C and l_1 coherence decrease to 0.135335 at t = 20, while fidelity decreases to 0.567668. At $\gamma = 0.5$, the corresponding final concurrence and coherence are 4.539993×10^{-5}, with fidelity 0.500023. At $\gamma = 1$, C and l_1 coherence are 2.061154×10^{-9} at t = 20, while fidelity is approximately 0.500000. The values at the largest dephasing rate are extremely small but are not mathematically zero at finite time. This distinction is retained in the reported values so that numerical resolution is not confused with the asymptotic limit. The characteristic coherence time, defined by the 1/e decay point, is $\tau d = 1/\gamma$, giving 10, 2, and 1 time units for $\gamma = 0.1$, 0.5, and 1.0, respectively.

The numerical integrity checks in Table 5 provide an independent assessment of the computed density matrices. Across the full simulation grid, the maximum closed-system normalization error is 8.882×10^{-16} and the maximum open-system trace error is 2.220×10^{-15}. Hermiticity is preserved to machine precision. The minimum eigenvalue encountered is -1.665×10^{-16}, which is a floating-point round-off value and is therefore consistent with positive semidefiniteness at the numerical precision of the calculation. These checks are important because the concurrence, coherence, and fidelity calculations are meaningful only when the underlying density matrices retain the required normalization and Hermiticity properties.

Table 5: Numerical Validation

Validation quantity	Numerical value	Interpretation
Maximum closed-system normalization error	8.882×10^{-16}	Numerically zero
Maximum open-system trace error	2.220×10^{-15}	Numerically zero
Maximum Hermiticity error	0	Zero within machine precision
Minimum density-matrix eigenvalue	-1.665×10^{-16}	Non-negative within numerical precision

The analytical benchmark in Table 6 gives a further, independent validation of the open-system calculation. The maximum discrepancies between numerical and analytical concurrence, l_1 coherence, and fidelity are all at the 10^{-15}–10^{-16} level for $\gamma = 0.1$, 0.5, and 1.0. Such differences are consistent with floating-point arithmetic and the specified solver tolerances rather than physical disagreement. The concurrence errors remain especially small despite the nonlinear eigenvalue-based concurrence evaluation, supporting the consistency of the numerical implementation. The simultaneous agreement of all three observables strengthens confidence that the dephasing term and the subsequent state analysis have been implemented consistently.

Table 6: Analytical Dephasing Benchmark

γ	Maximum C error	Maximum l_1-coherence error	Maximum F error
0.1	7.661×10^{-15}	4.996×10^{-16}	4.441×10^{-16}
0.5	1.998×10^{-15}	5.551×10^{-16}	5.551×10^{-16}
1.0	9.993×10^{-16}	3.886×10^{-16}	4.441×10^{-16}

Numerical convergence were examined by comparing representative trajectories obtained with progressively smaller internal step limits. As shown in Table 7, reducing the step limit from 0.02 to 0.01 and then from 0.01 to 0.005 changes concurrence by no more than 3.775×10^{-15}, while the corresponding changes in l_1 coherence and fidelity remain below 4.441×10^{-16} and 3.331×10^{-16}, respectively. Figure 6 provides the corresponding graphical summary of the convergence test. The very small differences indicate that further step refinement does not materially change the reported observables at the precision relevant to the study. The structural checks in Table 5 and the analytical benchmark in Table 6 establishes numerical stability of the reported results rather than just relying on visual agreement of trajectories alone.

Table 7: Numerical Convergence

Initial state	J	γ	Step comparison	Maximum $\lvert\Delta C\rvert$	Maximum $\lvert\Delta l_1\rvert$	Maximum $\lvert\Delta F\rvert$
$\lvert\Phi^+\rangle$	1	0.5	0.02 vs 0.01	2.220×10^{-15}	4.441×10^{-16}	3.331×10^{-16}
$\lvert\Phi^+\rangle$	1	0.5	0.01 vs 0.005	3.775×10^{-15}	4.441×10^{-16}	3.331×10^{-16}
Partial (p = 0.8)	1	1.0	0.02 vs 0.01	1.110×10^{-15}	4.441×10^{-16}	2.220×10^{-16}
Partial (p = 0.8)	1	1.0	0.01 vs 0.005	2.331×10^{-15}	4.441×10^{-16}	2.220×10^{-16}

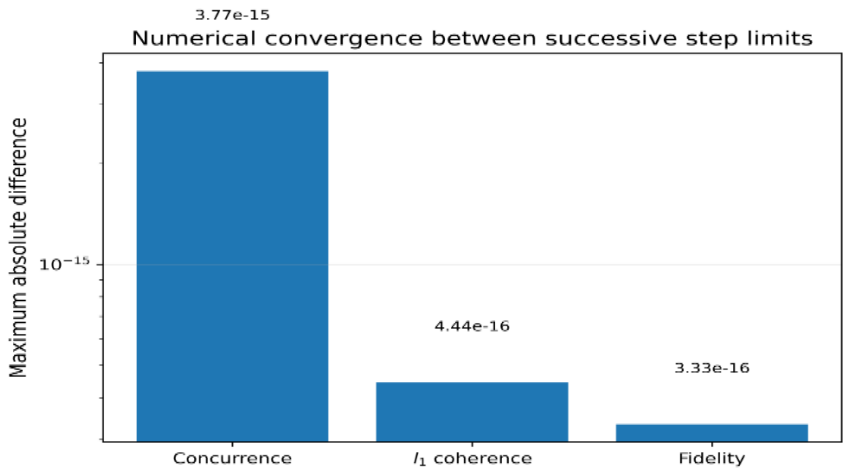

Figure 6: Numerical convergence between successive integration-step limits

The joint dependence of the partially entangled state on exchange coupling and dephasing is summarized by Figure 7 and Table 8. In the absence of dephasing, C (20) remains exactly 0.8000 across the entire tested J range. With $\gamma = 0.1$, the final concurrence is 0.10826823 for every J; increasing γ to 0.5 reduces it to 3.631994×10^{-5}, and $\gamma = 1$ reduces it to 1.648923×10^{-9}. The horizontal bands in Figure 7 therefore represent a genuine feature of the model rather than a plotting artefact: within the investigated parameter range, exchange coupling does not alter the final concurrence of this particular p = 0.8 state, whereas dephasing controls its loss. Figure 7 is consequently interpreted as a map of environmental suppression of an otherwise conserved closed-system concurrence. The result demonstrates that introducing exchange coupling alone does not increase the concurrence of the specified p = 0.8 state.

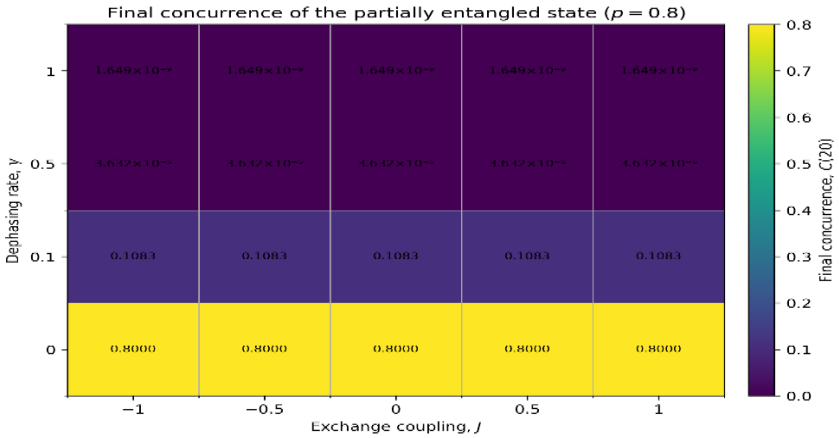

Figure 7: Final concurrence of the partially entangled state (p = 0.8) at t = 20 as a function of exchange coupling J and dephasing rate γ

Table 8: Final Concurrence for the Partial State (p = 0.8) at t = 20

γ	J = −1	J = −0.5	J = 0	J = 0.5	J = 1
0.0	0.80000000	0.80000000	0.80000000	0.80000000	0.80000000
0.1	0.10826823	0.10826823	0.10826823	0.10826823	0.10826823
0.5	3.631994×10^{-5}	3.631994×10^{-5}	3.631994×10^{-5}	3.631994×10^{-5}	3.631994×10^{-5}
1.0	1.648923×10^{-9}	1.648923×10^{-9}	1.648923×10^{-9}	1.648923×10^{-9}	1.648923×10^{-9}

The results distinguish coherent interaction effects from environmental decoherence. The isotropic Heisenberg interaction preserves the concurrence of the selected Bell benchmark and of the selected p = 0.8 state, while it can generate large transient entanglement from the separable $|01\rangle$ state. Local pure dephasing, in contrast, systematically suppresses off-diagonal coherence and consequently reduces both concurrence and fidelity. The three measures therefore provide complementary information: concurrence quantifies two-qubit entanglement, l_1 coherence tracks the magnitude of off-diagonal quantum coherence, and fidelity measures retention of the specified initial pure state. Their combined behaviour shows that high entanglement, high coherence, and high fidelity are related but not interchangeable properties of the evolving state. The quantitative validation also places the physical interpretation on a reproducible numerical basis. The full-grid normalization and trace errors are at machine-precision level, Hermiticity is preserved, the minimum eigenvalue remains at floating-point round-off level, the pure-dephasing trajectories agree with analytical expressions to approximately 10^{-15}–10^{-16}, and the step-refinement tests produce negligible changes. The conclusions are therefore specific to the Hamiltonian, initial states, Lindblad operators, and parameter ranges defined in Table 1. They should not be interpreted as universal properties of all Heisenberg spin systems or as direct experimental performance estimates. Real quantum devices may contain additional noise channels, control imperfections, calibration errors, and parameter scales outside the present model. Experimental calibration would consequently be required before translating these numerical benchmarks into hardware-specific performance claims.

CONCLUSION

This study addressed the problem of how coherent isotropic Heisenberg exchange and local Markovian pure dephasing affect two-qubit entanglement, quantum coherence, and fidelity for different initial-state classes. The numerical investigation was performed over $0 \leq t \leq$

20 for J = −1, −0.5, 0, 0.5, and 1 and γ = 0, 0.1, 0.5, and 1, using the four specified initial states. The results establish several state-dependent features of the model. The Bell state $|\Phi^+\rangle$ retains unit concurrence and fidelity under the closed isotropic interaction, while the partially entangled p = 0.8 state retains C = 0.8 for all tested exchange couplings. In contrast, the separable $|01\rangle$ state acquires strong transient entanglement through interaction, reaching concurrence values essentially equal to unity for |J| = 0.5 and 1, whereas the separable $|{+}{+}\rangle$ state remains unentangled to numerical precision. Thus, exchange coupling can create entanglement from a suitable separable state, but it does not universally increase the entanglement of an already entangled state.

The inclusion of local pure dephasing provides the environmental counterpart to the coherent interaction dynamics. For the Bell-state benchmark, concurrence and l_1-norm coherence follow the same exponential decay, $C(t) = l_1(t) = \exp(-\gamma t)$, while fidelity approaches 1/2 according to $F(t) = [1 + \exp(-\gamma t)]/2$. Increasing γ therefore accelerates the loss of coherence, entanglement, and fidelity. The p = 0.8 state shows the corresponding suppression of its preserved closed-system concurrence, with C (20) decreasing from 0.80000000 at γ = 0 to 1.648923×10^{-9} at γ = 1. The combined results show that interaction-induced entanglement generation and environmental decoherence are distinct mechanisms whose effects depend strongly on the initial state.

The computational results were additionally subjected to structural, analytical, and convergence validation. Across the full parameter grid, normalization and trace errors remained at machine-precision levels, Hermiticity was preserved, and the minimum density-matrix eigenvalue was consistent with positive semidefiniteness within floating-point precision. The Bell-state dephasing trajectories agreed with the analytical benchmark to approximately 10^{-15} to 10^{-16}, and successive step-refinement tests produced negligible changes in concurrence, l_1 coherence, and fidelity. These checks support the numerical reliability and reproducibility of the reported results. The study therefore solves the stated modelling problem by quantitatively separating exchange-driven coherent dynamics from dephasing-induced decoherence and by establishing validated numerical benchmarks for the selected Hamiltonian, Lindblad operators, initial states, and parameter ranges. The findings are model-specific and are not presented as experimentally calibrated device-performance estimates.

REFERENCES

Chatterjee, A., Stevenson, P., De Franceschi, S., Morello, A., de Leon, N. P., and Kuemmeth, F. (2021). Semiconductor qubits in practice. Nature Reviews Physics, 3, 157–177.

Chirolli, L., and Burkard, G. (2008). Decoherence in solid-state qubits. Advances in Physics, 57(3), 225–285.

Dirac, P. A. M. (1981). The Principles of Quantum Mechanics (4th Ed.). Oxford University Press.

Eisert, J., Friesdorf, M., and Gogolin, C. (2015). Quantum many-body systems out of equilibrium. Nature Physics, 11, 124–130.

Feynman, R. P. (1982). Simulating physics with computers. International Journal of Theoretical Physics, 21, 467–488.

Fu, Q., Wu, J., and Wang, X. (2024). Decoherence in exchange-coupled quantum spin qubit systems: Impact of multiqubit interactions and geometric connectivity. arXiv preprint arXiv:2401.00725.

Gebhart, V., Santagati, R., Gentile, A. A., Gauger, E. M., Craig, D., and Ares, N. (2023). Learning quantum systems. Nature Reviews Physics, 5, 141–156.

Heisenberg, W. (1928). Zur Theorie des Ferromagnetismus. Zeitschrift für Physik, 49, 619–636.

IBM Quantum. (2025). Quantum computing research and qubit technologies. IBM Research.

Landau, L. D., and Lifshitz, E. M. (1981). Quantum Mechanics: Non-Relativistic Theory (3rd Ed.). Pergamon Press.

Lutchyn, R. M., Cywinski, L., Nave, C. P., and Das Sarma, S. (2008). Quantum decoherence of a charge qubit in a spin-fermion model. Physical Review B, 78, 024508.

Microsoft Quantum. (2025). Scalable quantum computing systems. Microsoft Research.

Morsch, O., Palma, G. M., and Rossini, D. (2025). Quantum simulations of complex systems. La Rivista Del Nuovo Cimento, 48, 275–313.

Nielsen, M. A., and Chuang, I. L. (2010). Quantum Computation and Quantum Information. Cambridge University Press.

Obodo, K. O. (2024). Computational materials science and quantum technologies research contributions. University of KwaZulu-Natal Research Profile.

Preskill, J. (2018). Quantum computing in the NISQ era and beyond. Quantum, 2, 79.

Quantum Leap Africa. (2025). African-led quantum science and technology initiative. African Institute for Mathematical Sciences (AIMS).

Sachdev, S. (2011). Quantum Phase Transitions (2nd Ed.). Cambridge University Press.

Schlosshauer, M. (2019). Quantum decoherence. Physics Reports, 831, 1–57.

Yuan, S. (2010). Decoherence and thermalization of quantum spin systems. European Physical Journal B, 77, 423–438.